Computer-Aided Design 158 (2023) 103482

Contents lists available at ScienceDirect

Computer-Aided Design

journal homepage: www.elsevier.com/locate/cad

Explicit Tunnels and Cavities Control Using SIMP and MMA in Structural Topology Optimization

Tongxing Zuo, Haitao Han, Zhenyu Liu *

Changchun Institute of Optics, Fine Mechanics and Physics (CIOMP), Chinese Academy of Science, Changchun 130033, China
School of Optoelectronics, University of Chinese Academy of Sciences, Beijing 100049, China

ARTICLE INFO

Article history:
Received 27 July 2022
Received in revised form 9 December 2022
Accepted 24 January 2023

Keywords:
Topology optimization
Topological control
Topological invariants
Tunnel
Cavity
SIMP and MMA

ABSTRACT

The topology of a 3D continuum structure is usually characterized by the number of independent connected component and holes in the structure, where the holes include tunnels (through holes) and cavities (interior holes). The number of these features can be measured by the topological invariants of the structure (e.g., Betti numbers and Euler characteristic). The quantitative control of structural topology is important in topology optimization design because of various considerations, including design freedom, manufacturability, structural performance, and manufacturing costs. However, effective control of the structural topology during the topology optimization process remains a challenge, particularly to control the structural tunnels. To simplify the problem, only the number of tunnels (*NT*) and cavities (*NC*) of the structure are controlled in this paper. To solve the aforementioned problems, this study calculates the characteristic information of the tunnels and cavities by introducing the tunnel loops of homology theory and fire-burning method (FBM), while proposing a method for quantitative control of the 3D structural tunnels and cavities within the framework of the solid isotropic material with penalty (SIMP) interpolation of the design variable and method of moving asymptotes (MMA) optimization algorithm. The method achieves unilateral constraints over the structural tunnels and cavities by establishing explicit relationships between the element design variables in the structural topology optimization and *NT* as well as *NC* in the structure. Numerical examples demonstrate that the proposed method can effectively control the tunnels and cavities of an optimized structure.

1. Introduction

Topology optimization techniques are popular and powerful tools for maximizing the performance of a structure by optimizing its material layout. Several optimization techniques have been developed over the past three decades, including the homogenization [1], solid isotropic material with penalty [2], evolutionary structure optimization (ESO) [3], level set [4], moving morphable components (MMC) [5] and discrete variable [6] methods.

Although remarkable achievements have been made in the field of topology optimization, some challenges remain. One of these is the quantitative control of the structural topology. The topology of a 3D continuum structure is typically characterized by the number of independent connected component, tunnels (or handles), and cavities in the structure [7]. From a structural design perspective, the basic and most important idea is where to put the right holes [8]. Detailed information on the holes (i.e., position, number, shape, and feature size) determines the performance of the structure. Therefore, accurate control of the structural holes can provide designers with design freedom. In addition, multiple independent connected components may occur during topology optimization, thus it is necessary to control the number of independent connected components of the structure. From a traditional manufacturing perspective, the large holes in the structure means that the structure is more complex, and a more complex structure provides higher manufacturing energy consumption and time cost. Quantitative control over the structural holes is critical to selectively balancing the structural performance gains obtained by topology optimization design considering the manufacturing energy consumption and time cost and warrants further research. From an additive manufacturing (AM) perspective, although advanced AM techniques significantly reduce the cost related to structural complexity, cavities in the structure are undesirable for some processes such as selective laser sintering [9] and fused deposition modeling [10]. In summary, quantitative control over the structural topology in the topology optimization process has important theoretical and practical implications. To simplify the problem, only the *NT* and *NC* of the structure are controlled in this paper.

* Correspondence to: Changchun Institute of Optics, Fine Mechanics and Physics (CIOMP), Chinese Academy of Science, DongNanhu Road 3888, Changchun, Jilin, 130033, China.
E-mail address: liuzy@ciomp.ac.cn (Z. Liu).

https://doi.org/10.1016/j.cad.2023.103482
0010-4485/

Beginning with landmark filtering techniques that are used to eliminate numerical instabilities [11,12], there is a growing interest in controlling the structural topology of continuum structure in topology optimization. These filtering techniques can indirectly control the structural topology by changing the filter radius. For example, keeping other optimization parameters unchanged, the *NT* and *NC* obtained by using a larger filter radius is generally not greater than that obtained using a smaller filter radius. In addition to filtering techniques, various other techniques that can indirectly control the topology of the structure have been developed. Using the evolutionary structure optimization (ESO) method, Kim et al. [13] proposed an intelligent cavity creation (ICC) method that can indirectly control the *NC*. In addition, for skeleton-based [14] and geometric constraint methods [15] among others that can control the scale of the structure, generally, under the equality volume constraint, the larger the size of the structural features in the design domain is, the fewer the *NT* and *NC* in the structure. In contrast, the smaller the allowed structural feature size, the larger the *NT* and *NC* in the structure. Lu et al. [16] proposed a geometric constraint method for controlling cavities using the level set method. Based on the idea of analogous physical field solution characteristics, Li et al. [17], Liu et al. [18], and Yamada et al. [19] proposed a virtual temperature approach to eliminate cavities to fulfill the connectivity requirement.

Recently, scholars have developed a class of explicit direct methods for controlling the topology of structure. The idea to prescribe the *NC* for the structure has been adopted in a BESO-based approach [20]. In this approach, a hole-filling method was proposed to control the existence of cavities during the optimization process. Xiong et al. [21] developed an approach to controlling the structural cavities by generating tunnels Based on the graph theory and set theory. Zhao et al. [22] developed a direct approach to explicitly controlling the structural cavities during the form-finding process. This approach has been successfully applied to the morphological optimization of biological organs [23]. He et al. [24] proposed a boundary evolution method based on a thinning algorithm that which can keep the *NT* of the structure constant during the optimization. In the framework of discrete variable method and sequential approximate integer programming and canonical relaxation algorithm [25], Liang et al. [7] proposed an explicit formulation to calculate the *NC* based on the Euler–Poincaré formula and achieve the control of the *NC*. Han et al. [26] propose the quotient set design variable method to implement the inequality constraint on the maximum *NT* allowed in an optimized structure for 3D structural topology optimization. Under the SIMP method, Wang et al. [27] and Zuo et al. [28] both calculated the *NC* of 2D structure based on FBM [20] and achieved the control of *NC* based on persistent homology method and hole filling method, respectively.

Although topology control has been extensively studied in topology optimization, many details deserve further investigation. For example, implicit indirect methods cannot quantitatively control structural topology. Explicit direct methods can quantitatively control the structural topology, but some of these approaches are limited to 2D optimization. Xiong et al. [21], Zhao et al. [22] and Liang et al. [7] did not discuss tunnels with 3D structures. Although the method proposed by He et al. [24] can control the tunnels, it relies on a fixed topological configuration. Though Han et al. [26] achieved inequality control of the *NT* based on boundary evolution, the efficiency of boundary evolution is relatively low. Therefore, the development of more effective explicit quantitative topological control methods is still of interest, especially in the framework of the most general combination of SIMP interpolation and MMA optimization algorithm [29].

In this study, 3D tunnels and cavities control combining SIMP interpolation and MMA optimization algorithm is proposed based on 2D topology control work [28]. Compared to the 2D topology control work, the core difficulty is to calculate the characteristic information of the 3D structural tunnels. Holes in 2D structure have only one type, namely cavity, which can be described as a void area that is surrounded by solid elements. However, holes in 3D structure contain two types, i.e., cavity and tunnel, where the tunnel is not enclosed by solid elements. The following is the research idea of 3D topological control. Because the description of the independent connected components, tunnels, and cavities depends on the binarized structure (BS), it is not possible to directly define the independent connected component, tunnels and cavities of the structure with gray elements (SGE). Therefore, the first step was to project the SGE into the BS. The BS may have nonmanifold points and nonmanifold edges [30,31]. These behave as 1-node connected hinges and 1-edge connected hinges, respectively, in the structural topology optimization. The object of study in this paper is manifold. In other words, this paper only researches the structure without nonmanifold points and nonmanifold edges. Therefore, it is necessary to eliminate the nonmanifold points and nonmanifold edges in each iteration. Poulsen et al. [32] and Liang et al. [7] effectively handled nonmanifold points and nonmanifold edges for a structured hexahedral mesh. The method of Liang et al. [7] is used in this study to deal with nonmanifold points and nonmanifold edges.

After obtaining the manifold binarized structure (MBS), in other words, after obtaining the binarized structure without nonmanifold points and nonmanifold edges, the second step is to calculate the independent connected components, tunnels, and cavities of the MBS. The number of these features can be measured using topological invariants of the structure (e.g., Betti numbers and Euler characteristic). However, topological invariants do not provide detailed information regarding these features. Therefore, in this study, detailed information on these features was calculated using the FBM and tunnel loops of homology theory [33,34]. The independent connected components, tunnels, and cavities of the MBS are used to describe the topological characteristics of the corresponding SGE. The third step is to control the structural topology by introducing a topological constraint into the SIMP-based optimization model. This topological constraint and corresponding sensitivity establish an explicit relationship between the element design variables and *NT* as well as *NC* in the MBS. Finally, the element design variables are updated using the MMA optimization algorithm. The remainder of this paper is organized as follows. The problem statement is presented in Section 2. In Section 3, the *NT* and *NC* of the MBS are calculated based on Betti numbers, Euler characteristic, and FBM. The discrete topology constraint and control method for the topology are presented in Section 4. Section 5 presents the optimization framework for controlling the structural topology. Three 3D numerical examples are presented in Section 6. The paper ends with concluding remarks in Section 7.

To facilitate the readability of this manuscript, we provide Table 1 to summarize the acronyms and corresponding extended definitions.

2. Problem statement

The topology of a 3D continuum structure is characterized by its number of independent connected component and holes, where the holes include tunnels (through holes) and cavities (interior holes). In this paper, we use T_i, $1 \leq i \leq NT$ and C_i, $1 \leq i \leq NC$ to denote the tunnels and cavities, respectively. As in Fig. 1(a), there are two tunnels and one cavity. In mathematical topological analysis, the number of independent connected component and holes of a geometric entity can be measured in terms of its topological invariants. To simplify the problem, only *NT* and *NC* of the structure are controlled in this paper.

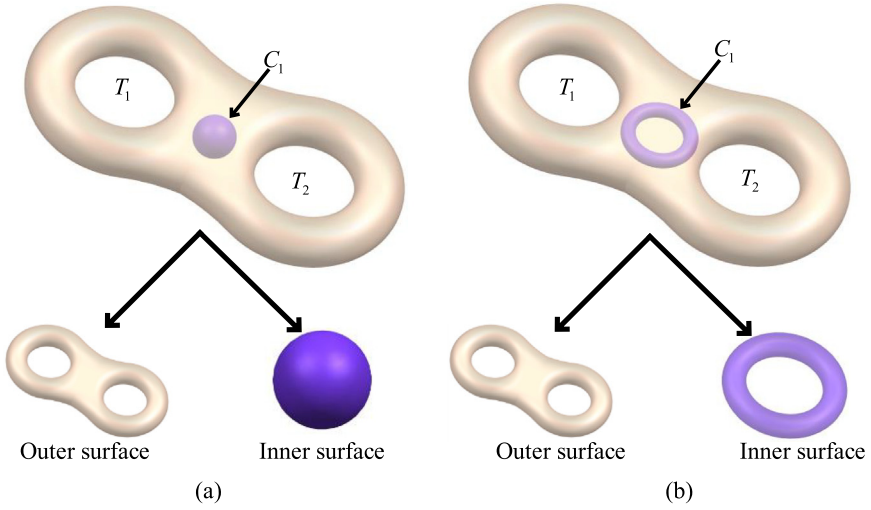

Fig. 1. Schematic of 3D structural cavities affecting *NT* computation.

Table 1
Acronyms and corresponding extended definitions.

	Acronyms	Extended definitions
1.	SIMP	Solid isotropic material with penalty
2.	MMA	Method of moving asymptotes
3.	ESO	Evolutionary structure optimization
4.	BESO	Bi-directional evolutionary structural optimization
5.	AM	Additive manufacture
6.	GA	Genetic algorithm
7.	ICC	Intelligent cavity creation
8.	HFM	Hole-filling method
9.	BS	Binarized structure
10.	SGE	Structure with gray elements
11.	*TCS*	Topological constraint set
12.	*SNPE*	A set of elements to be processed to eliminate nonmanifold points and edges
13.	OC	Optimality criteria
14.	*NT*	Number of tunnels
15.	*NC*	Number of cavities
16.	MBS	Manifold binarized structure
17.	FBM	Fire-burning method
18.	EC_i	Elements contained in *i*th cavity
19.	ET_i	Elements contained in *i*th tunnel
20.	S_i	*i*th solid connected subdomain
21.	V_i	*i*th void connected subdomain
22.	V_Ω	Background mesh

In present work, the topology optimization problem under consideration is to minimize or maximize the structural objective function value under the structural topological inequality constraint. In the SIMP framework, the optimization problem can be formulated as follows:

$$\begin{aligned} &\text{Find } \boldsymbol{\rho} = (\rho_1, \rho_2, \ldots, \rho_n)^{\mathrm{T}} \\ &\text{Min } C(\boldsymbol{\rho}) \text{ or Max } C(\boldsymbol{\rho}) \\ &\text{S.t. } \boldsymbol{K}(\rho)\boldsymbol{u} = \boldsymbol{f} \\ &\quad V(\boldsymbol{\rho}) = \sum_{i=1}^{n} \rho_i v_i / \sum_{i=1}^{n} v_i \le \overline{\mathrm{V}} \\ &\quad \rho_{\min} \le \rho_i \le 1, \forall i \in 1, 2, \ldots, n \\ &\quad NT(\boldsymbol{\rho}) \le \overline{\mathrm{NT}} \\ &\quad NC(\boldsymbol{\rho}) \le \overline{\mathrm{NC}} \end{aligned} \tag{1}$$

In Eq. (1), $\boldsymbol{\rho}$ is the vector of the element design variables, with ρ_i and v_i denoting the value and volume of the *i*th element. The symbol n denotes the total number of finite elements used to discretize the prescribed design domain Ω. C is an objective function. $\boldsymbol{K} = \sum_{i=1}^{n} \rho_i^p \boldsymbol{K}_0$ (p is the penalization index, and $p = 3$ is adopted in the present study) is the global stiffness matrix, with $\boldsymbol{K}_0$ representing the element stiffness matrix corresponding to $\rho_i = 1$. $\boldsymbol{f}$ and $\boldsymbol{u}$ are the external load and displacement fields, respectively. $\overline{V}$ is the prescribed upper bound for a solid material. $\underline{\rho_{min}}$ is the lower bound of the element design variable. $NT(\boldsymbol{\rho}) \le \overline{NT}$ and $NC(\boldsymbol{\rho}) \le \overline{NC}$ are topological constraints, where $\overline{NT}$ and $\overline{NC}$ represent the maximum constraint numbers of tunnels and cavities, respectively. Therefore, in this study, three modes were used to control 3D structural tunnels and cavities. The first is to control only the structural tunnels, that is $NT(\boldsymbol{\rho}) \le \overline{NT}$. The second is to control only the structural cavities, that is, $NC(\boldsymbol{\rho}) \le \overline{NC}$. The third is to control both the structural tunnels and cavities, that is $NT(\boldsymbol{\rho}) \le \overline{NT}, NC(\boldsymbol{\rho}) \le \overline{NC}$.

3. Measure the structural cavities and tunnels

How to measure the *NT* and *NC* of 3D geometrical entities is a great research topic of mathematical topology analysis. The topology analysis concentrates on the invariants under the continuous deformation of the geometrical entity, e.g., the Euler characteristic and Betti numbers.

For the 3D geometrical entity as shown in Fig. 1, the Euler characteristic χ can be expressed as follows:

$$\chi = n_0 - n_1 + n_2 - n_3 \tag{2}$$

where n_0, n_1, n_2, and n_3 represent the number of vertices, edges, faces, and elements, respectively. The relationship between the Euler characteristic χ and the Betti numbers B_0, B_1, B_2 is:

$$\chi = B_0 - B_1 + B_2 \tag{3}$$

where the Betti number B_0, is the number of the independent connected component, the Betti number B_1 is the sum of the *NT* of the 3D geometric entity and the *NT* of its extracted solidified independent cavities, and the Betti number B_2 is the *NC*. It can be seen that the *NT* calculation of a 3D geometric entity is influenced by the topological information of its cavities. For example, a simply connected 3D geometric entity as shown in Fig. 1(a) has two tunnels T_i, $1 \le i \le 2$ and a cavity C_1 without tunnels, thus its three Betti numbers are $B_0 = 1$, $B_1 = 2$, and $B_2 = 1$. A simply connected 3D geometric entity as shown in Fig. 1(b) has two tunnels T_i, $1 \le i \le 2$ and a cavity C_1 with a tunnel, thus its three Betti numbers are $B_0 = 1$, $B_1 = 3$, and $B_2 = 1$. Therefore, the *NT* in a 3D structure cannot be measured directly using B_1.

Multiple independent connected components may occur during topology optimization. Therefore, in this paper, the strategy to calculate *NT* and *NC* of geometric entities is to first calculate all independent connected components S_i, $1 \le i \le ns$, where ns is the number of independent connected components. Then the NC_i, $1 \le i \le ns$ is calculated for each independent connected component. The *NC* for geometric entities is

$$NC = \sum_{1 \le i \le ns} NC_i \tag{4}$$

Before calculating the *NT*, the whole cavities of the structure are filled as solids. In this way, the three Betti numbers for each independent connected component can be expressed as $B_0 = 1$, $B_1 = NT_i$ and $B_2 = 0$. Therefore, according to Eqs. (2) and (3), the number of tunnels in the *i*th independent connected component without cavities can be calculated.

$$NT_i = B_1 = B_0 + B_2 - n_0 + n_1 - n_2 + n_3 = 1 - n_0 + n_1 - n_2 + n_3 \tag{5}$$

The *NT* for geometric entity is

$$NT = \sum_{1 \le i \le ns} NT_i \tag{6}$$

The definition of an independent connected components, tunnels, and cavities is dependent on the BS. However, in the framework of the SIMP method, gray elements inevitably appear in the structure. In addition, nonmanifold points and nonmanifold edges may appear in the BS. However, this paper only study structure without nonmanifold points and nonmanifold edges. Therefore, three problems must be addressed to identify cavities and tunnels during the optimization. First, a method should be defined to project the continuous design variable to 0–1 to obtain the BS. Second, the nonmanifold points and nonmanifold edges in BS are processed to obtain MBS. Finally, a numerical algorithm is applied to calculate the cavities and tunnels in the MBS. The main flowchart for calculating the cavities and tunnels of the MBS is shown in Fig. 2.

3.1. Projecting SGE to BS

To obtain the BS, a straightforward approach is to project the continuous value of the design variables $\rho \in [\rho_{min}, 1]$ to the discrete 0–1 design variables. There are many algorithms for implementing projection operations [35–40]. We adopted Wang's projection strategy [27] for this study. This strategy consisted of two separate steps. The first step is to calculate the threshold $\overline{\rho}$ using the classical OC algorithm under the volume equation constraint, and the second step is to map the design variables greater than the threshold to 1 and to 0 otherwise. Thus, the 0–1

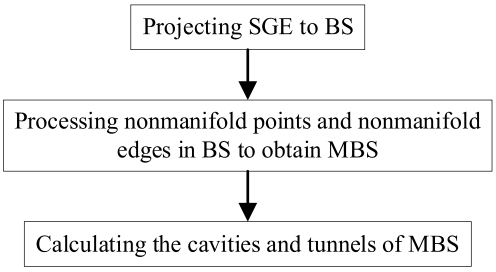

Fig. 2. Main flow chart for calculating cavities and tunnels.

design variable $\hat{\boldsymbol{\rho}}$ is obtained. At each iteration of the optimization process, the volume preservation projection method ensures that the variables satisfy the following formula:

$$\begin{aligned} &\hat{\rho}_i = \begin{cases} 1, \rho_i > \overline{\rho} \\ 0, \rho_i \le \overline{\rho} \end{cases} \\ &\sum \hat{\rho}_i v_i = \sum \rho_i v_i \end{aligned} \tag{7}$$

where ρ_i and v_i denote the design variable value and volume of the *i*th element, respectively. Fig. 3(a) shows the SGE for one iteration. Fig. 3(b) shows the BS obtained by projecting according to a given threshold $\overline{\rho} = 0.5$, where $\overline{V} = 0.12$. Fig. 3(c) shows the BS obtained by volume preservation projection under the condition of volume fraction $\overline{V} = 0.12$, where $\overline{\rho} = 0.5038$.

3.2. Fire-burning method

The identification of nonmanifold points and nonmanifold edges as well as the calculation of tunnels and cavities in the paper require the partitioning of the mesh by the FBM. This section provides a detailed description of the FBM.

In this paper, the mesh element is denoted by $e \in V_\Omega = S_i \cup V_j$, $1 \le i \le ns$, $1 \le j \le nv$, where V_Ω, S_i, V_j, ns and nv denote the background mesh, solid connected subdomains, void connected subdomains, the number of solid connected subdomains and the number of void connected subdomains, respectively. Two pieces of information are required to divide the mesh into connected subdomains using FBM, one is the property of mesh (e.g., discrete variable value) and the other is information about the mesh neighbors. The objects studied in this paper do not allow for nonmanifold points and nonmanifold edges, thus the face-neighbors *FN* (*e*) of the mesh element *e* shown in Fig. 4 is used. Two mesh elements e_i and e_j belong to the same connected subdomain if they satisfy the following equation:

$$\begin{cases} e_i \in FN\left(e_j\right) \\ \hat{\rho}\left(e_i\right) = \hat{\rho}\left(e_j\right) \end{cases} \tag{8}$$

Based on the above two pieces of information, the detailed procedure for calculating all elements contained in the connected subdomain using FBM is shown in Table 2.

3.3. Handling nonmanifold points and nonmanifold edges

Nonmanifold points and nonmanifold edges may be present in the BS. From a geometric point of view, a nonmanifold point and nonmanifold edge refer to solid elements (elements with design variable 1) connected by only one node and one edge, respectively. The nonmanifold points and nonmanifold edges in the structural topology optimization behave as 1-node connected hinges and 1-edge connected hinges, respectively. For example, the blue point in Fig. 5(a) is a nonmanifold point, and the blue edge in Fig. 5(b) is a nonmanifold edge. However, this paper only

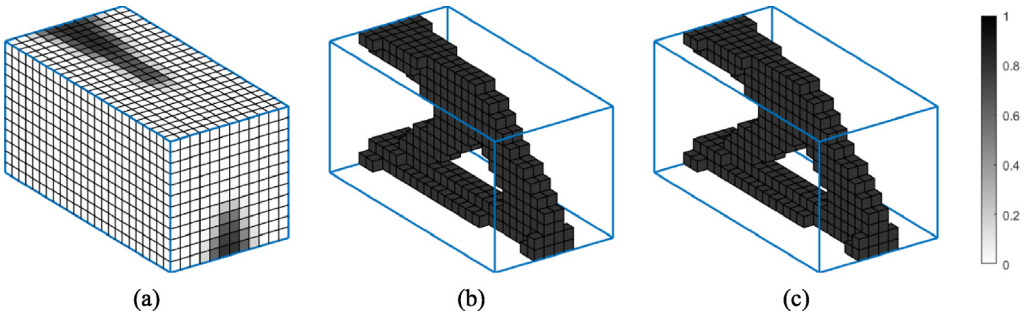

Fig. 3. Schematic of the projection with a threshold of 0.5 and the volume preservation projection.

Table 2
Algorithm for calculating connected subdomains with FBM.

Algorithm 1:

Input: V_Ω
1. Define the connected subdomain *CS* and fire-burning set *fire*.
2. Select an arbitrary element from V_Ω. Label it and add it to *fire* and *CS*.
3. **while** *fire* is not empty
4. Takes the first element *fp* of *fire* and removes it from *fire*.
5. **for** $m = 1$ **to** the number of *FN*(*fp*)
6. **if** the value of the current element is equal to that of *fp* and is not labeled
7. label it and add it to both *fire* and *CS*.
8. **end**
9. **end**
10. **end**

Output: A connected subdomain *CS* of V_Ω

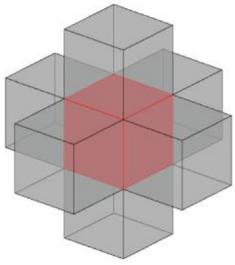

Fig. 4. The shaded elements are the face-neighbors $FN(e)$ of the red element e at the center. (For interpretation of the references to color in this figure legend, the reader is referred to the web version of this article.)

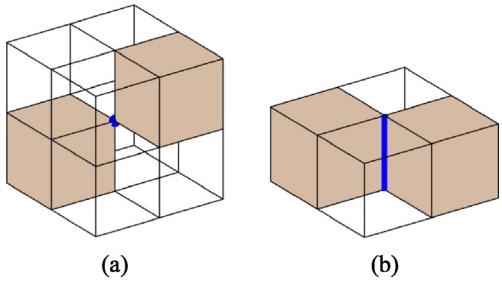

Fig. 5. Schematic of the nonmanifold point and the nonmanifold edge. (For interpretation of the references to color in this figure legend, the reader is referred to the web version of this article.)

study structure without nonmanifold points and nonmanifold edges. Therefore, it is best to eliminate all nonmanifold points and edges completely in each iteration. The set of adjacent elements EP_i for the ith point p_i of the mesh is defined as:

$$EP_i = \left\{ e_j | p_i \in PE_j \right\} \tag{9}$$

Where PE_j represents the set of points of the jth element e_j. Use Algorithm 1 to calculate the solid connected subdomains of EP_i. If the number of its solid connected subdomains is greater than 1, then the p_i is a nonmanifold point. The method of identifying nonmanifold edges is similar to the method of identifying nonmanifold points.

Typically, the nonmanifold points and nonmanifold edges can be eliminated by using a sufficiently large filter radius. However, there is no predefined quantitative method for choosing an appropriate filter radius. In this paper, the strategy for dealing with nonmanifold points and nonmanifold edges is to change the void elements (elements with design variable 0) that are adjacent to the nonmanifold points and nonmanifold edges in the BS to solid elements, marking the set consisting of these void elements eliminating nonmanifold points and edges in BS as *SNPE*, and then adding *SNPE* to the topological constraint set (TCS). The purpose of adding the *SNPE* to the *TCS* is to update their values with a target of 1 according to the MMA, thus achieving the suppression of 1-node connected hinges and 1-edge connected hinges in the SGE. This article uses the algorithm of Liang et al. [7] to calculate the *SNPE*.

3.4. Calculating the NC and NT

As described at the beginning of Section 3, the number of B_1 in a 3D structure is affected by the cavity. To avoid the influence of the cavity in the structural tunnel calculations, this study calculates the cavities and tunnels based on Betti numbers, Euler characteristic, and FBM.

During the optimization process, the MBS obtained after volume preservation projection may be multiconnected. The calculation of *NT* and *NC* consists of the following steps.

Step 1. The solid and void connected subdomains S_i, $1 \le i \le ns$ and V_j, $1 \le j \le nv$ of the MBS are calculated according to the FBM.

Step 2. Calculate the surface meshes SS_i, $1 \le i \le ns$ and SV_j, $1 \le j \le nv$ for S_i, $1 \le i \le ns$ and V_j, $1 \le j \le nv$, respectively.

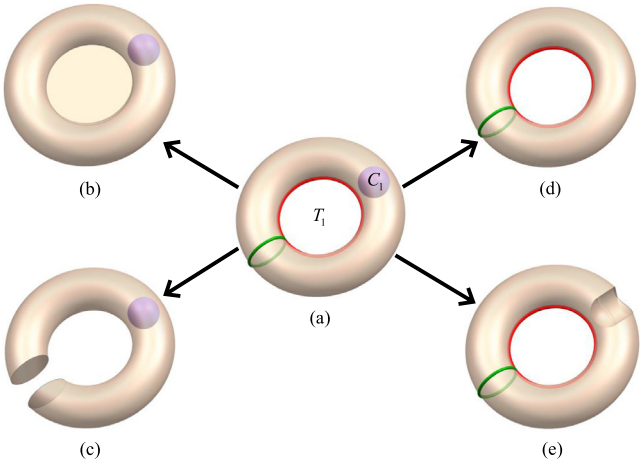

Fig. 6. Schematic diagram of the reduction of structural cavities and tunnels according to the filling and cutting methods, respectively. (For interpretation of the references to color in this figure legend, the reader is referred to the web version of this article.)

Step 3. Traverse SS_i, if $SV_j \subseteq SS_i$ exists, then V_j is a cavity. Denote these cavities by EC_i, $1 \leq i \leq NC$, where EC_i denotes the set of elements contained in the ith cavity.

Step 4. Fill all cavities of MBS as solids so that S_i, $1 \leq i \leq ns$ have no cavities. Then the NT of MBS was calculated according to Eqs. (5) and (6).

4. Control structural tunnels and cavities

There are two methods to reduce the NT and NC, one is the filling method, which is to fill the tunnels and cavities of the structure as solids. For example, the tunnel and cavity of the structure shown in Fig. 6(a) are filled as solids shown in Fig. 6(b) and (d), respectively. The other is the cutting method, in which the solid structures around the tunnels and cavities are sheared apart. For example, the solid structure of the tunnel and cavity shown in Fig. 6(a) is cut into the solids shown in Fig. 6(c) and (e), respectively. In this paper, the tunnels and cavities of the structure are controlled by the filling method.

For the case where topological constraints in Eq. (1) are not satisfied, the tunnels and cavities of the structure must be controlled according to the set of elements contained in the tunnels and cavities. The set of elements contained in each cavity EC_i, $1 \leq i \leq NC$ has been calculated in Section 3.4, but the set of elements contained in the tunnels ET_i, $1 \leq i \leq NT$ is still unknown. In this study, there are two requirements for the set of elements contained in the tunnels: one is that the intersection of the set of elements contained in the tunnels should be as small as possible to reduce the mutual influence between the tunnels, and the ideal state is that there is no intersection; the other is that the tunnels should contain as few elements as possible because constraining more elements may lead to topological constraint that are difficult to satisfy smoothly. In order to satisfy the above requirements, this paper calculates the ET_i, $1 \leq i \leq NT$ based on the triangular meshing of the 3D polygons and tunnel loops (3D polygons) in the homology theory.

4.1. Discrete topological constraint

The control of tunnels and cavities is realized by adding a topological constraint to the framework of the SIMP interpolation of the design variable and MMA optimization algorithm.

The $NT \leq \overline{NT}$ and $NC \leq \overline{NC}$ in Eq. (1) are integrated as a topological constraint with the following discretized form.

$$tc(\boldsymbol{\rho}) = \sum_{j \in TCS} \left(\rho_j - 1\right)^2 \leq \varepsilon \tag{10}$$

In Eq. (10), TCS is the topological constraint set such that

$$TCS = \left\{ i | i \in \{1, \ldots, n\}, \rho_i \in \cup_{1 \leq j \leq NT - \overline{\mathrm{NT}}} ET_j \cup_{1 \leq k \leq NC - \overline{\mathrm{NC}}} EC_k \right\} \tag{11}$$

where n denotes the total number of finite elements used for discretizing the prescribed design domain. ET_j and EC_k denote the set of elements contained in the jth tunnel and the set of elements contained in the kth cavity, respectively. NT and NC denote the number of tunnels and cavities, respectively. $\overline{NT}$ and $\overline{NC}$ refer to the maximum constraint number of tunnels and cavities, respectively. As shown in Fig. 7, the maximum constraint numbers of tunnels and cavities are both zero, that is, $\overline{NT} = \overline{NC} = 0$. However, the number of tunnels and cavities of the MBS are both one, that is, $NT = NC = 1$. The sets of elements (red elements) contained in the tunnel and cavity are denoted as ET_1 and EC_1, respectively. Therefore, both ET_1 and EC_1 need to be added to TCS to realize topological constraint. The sensitivity of the topological constraint is expressed as

$$\frac{\partial tc}{\partial \rho_i} = \begin{cases} 2 * (\rho_i - 1) \leq 0, i \in TCS \\ 0, i \notin TCS \text{ and } i \in \Omega \end{cases} \tag{12}$$

Therefore, the element design variables can be updated simultaneously by considering multiple constraints, including topological inequality constraint using the MMA optimization algorithm.

4.2. Definition and calculation of tunnel loops and handle loops

In order to give a precise control of the structural tunnels, it is necessary to define the tunnels in a mathematical rigorous way. In the following, this will be achieved by introducing the concept of tunnel loops on the outer surface of a given structure. Let M be the outer surface of a structure which is a connected, closed (compact and without boundary), orientable, and embedded in R^3. The genus of M represents the maximum number of cuttings along nonintersecting closed simple curves achievable without disconnecting M. The M partitions R^3 into two regions, I and O, where $I \cap O = M$ and $I \cup O = R^3$. The unbounded region O is called the exterior of M, whereas the bounded region I is the interior of M. Based on the work of Dey et al. [41] we can define the tunnel loop and handle loop as follows:

Definition 1 (*Tunnel Loop*)**.** A loop on M is a tunnel loop if it is trivial in O but nontrivial in I.

Definition 2 (*Handle Loop*)**.** A loop on M is a handle loop if it is trivial in I but nontrivial in O.

As shown in Fig. 6, the green loop can be continuously reduced to a point in I, but not in O, hence the green loop is a handle loop; similarly, the red loop can be continuously reduced to a point in O, but not in I, hence the red loop is a tunnel loop. It is worth noting that a handle loop necessarily corresponds to a tunnel loop and vice versa. In addition, the initial tunnel loop may not have an ideal geometry; specifically, it may be unnecessarily overlong and twisted. Therefore, the shortest length constraint must be added to the tunnel loop to obtain the shortest tunnel loop. The red loops in Figs. 6 and 8 are the shortest tunnel loop. For structures with complex topologies, the tunnel loops may differ from general geometric intuition. As shown in Fig. 8, the surface does not separate after cutting along the three red curves, but if cutting is continued along the blue curve, the surface will split into two parts. Thus, the genus of this surface is 3, which

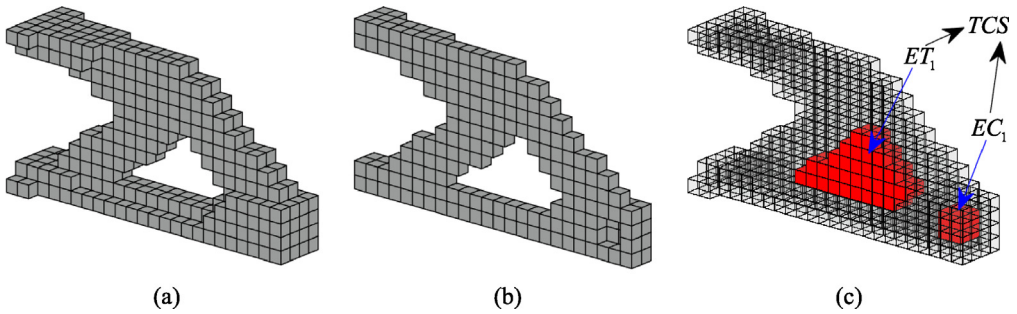

Fig. 7. Demonstrate the topological constraint set *TCS*, where opaque (a), half (b) and semi-transparent (c) versions of the structure are used for visualization. (For interpretation of the references to color in this figure legend, the reader is referred to the web version of this article.)

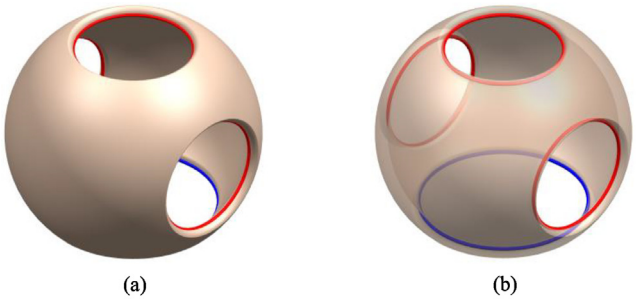

Fig. 8. A group of shortest tunnel loops on a surface, where opaque (a) and semitransparent (b) versions of the surface are used for visualization. (For interpretation of the references to color in this figure legend, the reader is referred to the web version of this article.)

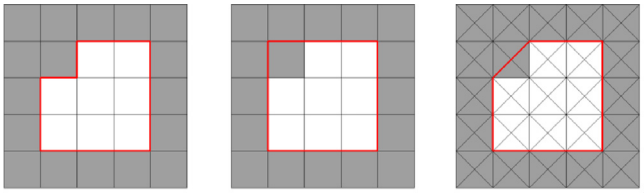

Fig. 9. Multisolution of the shortest tunnel loop position. (For interpretation of the references to color in this figure legend, the reader is referred to the web version of this article.)

means that the surface has three tunnel loops. Notably, any three of the four loops in Fig. 8 can be selected as a group of tunnel loops, but under the constraint of the shortest length, the three red curves are a group of shortest tunnel loops of the surface, which naturally reduces the multisolvability.

In this paper, the outer surface of the independent connected component is a discrete structured quadrilateral mesh; thus, there may be multiple sets of shortest tunnel loops on this surface that are equal in length but differ in spatial location. To ensure uniqueness, this study triangulates the quadrilateral mesh based on the two diagonals of the quadrilateral and calculates the shortest tunnel loops based on the triangular mesh. As in the left and middle two figures of Fig. 9, they are both the same quadrilateral mesh, but the two shortest tunnel loops (red loops) obtained are at different locations, and after triangular meshing of the quadrilateral mesh, only the shortest tunnel loop (red loop) is obtained, as shown on the right side of Fig. 9. In this study, tunnel loops are calculated using Dey et al.'s algorithm [34].

4.3. Calculate the set of elements contained in the tunnel

Once the shortest tunnel loops have been computed in Section 4.2, the triangulating 3D polygons algorithm [42] can be adopted to find the triangular mesh with the minimum area bounded by each tunnel loops (3D polygons) as a boundary. For the sake of completeness, the basic ideas of this algorithm will be explained as follows. Each shortest tunnel loop consists of a sequence of points $TL_i = \left\{p_j | 1 \le j \le n, p_j \in R^3\right\}$, $1 \le i \le NT$, where n is the number of points in the ith tunnel loop. Define a weight function

$$WF : TL_i^3 \to L_{area} = [0, \infty) \tag{13}$$

Where $TL_i^3 = \{p_m, p_n, p_k\}$ is a triangle constructed from any three points in TL_i, WF assigns an area to each triangle TL_i^3, and L_{area} is the sum of the areas of all the triangles formed by TL_i. Finally, the triangular mesh with TL_i as the boundary is calculated according to the algorithm of Dey et al. [42] which minimizes L_{area}. Then, the void elements are taken on the background mesh intersecting each triangular mesh as the set of elements contained in the corresponding tunnel ET_i, $1 \le i \le NT$.

The flow for calculating the set of elements contained in the tunnel of an independently connected component is illustrated in Fig. 10. The surface quadrilateral mesh of an independently connected component without a cavity is shown in Fig. 10(a). Fig. 10(b) shows the surface triangular mesh of the independent connected component and one of the shortest tunnel loops. Fig. 10(c) shows one of the shortest tunnel loops. Fig. 10(d) shows the triangular mesh generated with the shortest tunnel loop shown in Fig. 10(c) as the boundary. Fig. 10(e) shows the void element (yellow element) on the homogeneous mesh that intersects the triangular mesh shown in Fig. 10(d). Fig. 10(f) shows the set of elements contained in the tunnel (yellow elements).

4.4. Strategies for controlling NT and NC

When controlling the tunnels and cavities of the structure it may occur that the regions where the tunnels and cavities were reduced by topological constraint in the previous iterations generate new tunnels and cavities in the subsequent topological optimization process. To solve the above problem, we use boundary evolution to update the TCS.

For any element $e \in V_\Omega$, it belongs to the set of the boundary elements ∂S_i of S_i if it satisfies the following condition:

$$e \in S_i \text{ and } FN(e) \cap \left(\cup_{1 \le j \le nv} V_j\right) \ne \varnothing \tag{14}$$

In addition, when controlling the tunnels of S_i, further processing of ∂S_i is needed to prevent the NT of S_i from increasing when deleting arbitrary boundary elements. The detailed procedure for processing ∂S_i is shown in Table 3. As shown in Fig. 11, all solid elements of the given structure are boundary elements. If the red solid elements are changed to void elements, the NT of the structure increases.

In this study, the element design variables are updated based on MMA to reduce NT and NC by adding the selected set of

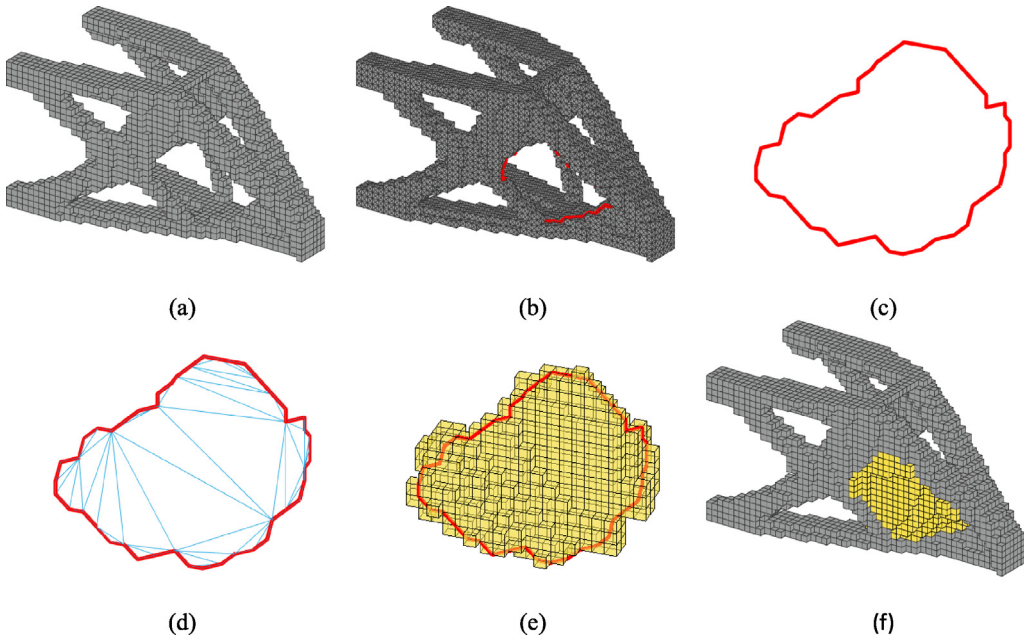

Fig. 10. Flowchart showing the calculation of the set of elements contained in corresponding tunnel. (For interpretation of the references to color in this figure legend, the reader is referred to the web version of this article.)

Table 3
Algorithm for processing the set ∂S_i of boundary elements of S_i.

Algorithm 2:
Input: V_Ω, S_i, ∂S_i
Calculate the B_1 of S_i according to Eqs. (2) and (3).
for $k = 1$ **to** number of elements contained in ∂S_i **do**
Assign S_i to the temporary elements set ST_i.
Change the elements in ST_i corresponding to the kth element and its FN to the void elements. Then calculate the B_1^k of ST_i according to Eqs. (2) and (3).
if $B_1^k - B_1 = 1$
Remove the current element from ∂S_i.
end
end
Output: ∂S_i

elements contained in the tunnel ET_i and cavity EC_i to TCS. However, this approach may severely affect the topology optimization process because the controlled tunnels and cavities contain regions that are too large, including topological constraint, which make it difficult to smoothly satisfy the constraint. To solve this problem, this study controls NT and NC using the following strategy. First, the tunnels and cavities are arranged in ascending order according to their contained regions as $ET_i, 1 \le i \le \overline{NT}$ and $EC_i, 1 \le i \le NC$, respectively. Then $ET_i, 1 \le i \le NT - \overline{NT}$ and $EC_i, 1 \le i \le NC - \overline{NC}$ are added into TCS. Notably, other strategies can be used to sort the tunnels and cavities, such as sorting tunnels and cavities based on the sensitivity sum of the elements they contain. A more general discussion of this point is not extended in this study.

To suppress the phenomenon in which the regions where the tunnels and cavities were reduced by the topology constraint in the previous iterations generate new tunnels and cavities in the subsequent topology optimization process, the detailed implementation is divided based on the following two cases. The first case occurs where the current iteration does not satisfy the topological constraint. In this case, instead of initializing TCS to empty, the intersection of TCS with the updated MBS boundary element set is removed from TCS. The updated MBS is obtained by filling selected tunnels $ET_i, 1 \le i \le NT - \overline{NT}$ and cavities $EC_i, 1 \le i \le NC - \overline{NC}$ in the MBS as solids, and then performing nonmanifold points and nonmanifold edges processing. In the second case, the topological constraint is not satisfied in the previous iteration but is satisfied in the current iteration. In this case, TCS is first changed to empty, and all the solid elements of the MBS except the boundary elements are then added to TCS. The set of boundary elements of the MBS must be further processed in the control structure tunnels using Algorithm 2.

5. Optimization framework

In summary, the algorithm in this study first binarized the SGE to BS. Then, the nonmanifold points and nonmanifold edges of the BS are processed to obtain the MBS. Subsequently, the tunnels and cavities of the MBS are analyzed, and the topology of the SGE is described using the tunnels and cavities of the MBS. For cases in which the topological constraint is not satisfied, such as $NT > \overline{NT}$ or $NC > \overline{NC}$, the specified set of elements contained in the tunnels or cavities are selected to join the TCS, and the element design variables are updated based on the MMA algorithm to achieve the NT or NC reduction. Moreover, one of the basic features of topology optimization is the generation of tunnels and cavities. In this study, a boundary evolution strategy is used to control the generation of new tunnels and cavities for the two cases of the structure not satisfying topological constraint and structure satisfying topological constraint after topological

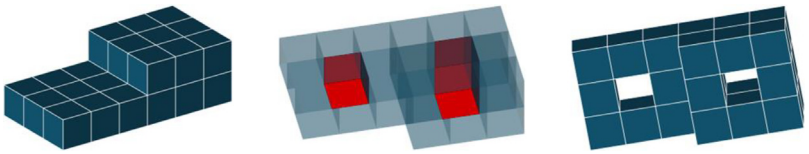

Fig. 11. Solid boundary elements that can change *NT*. (For interpretation of the references to color in this figure legend, the reader is referred to the web version of this article.)

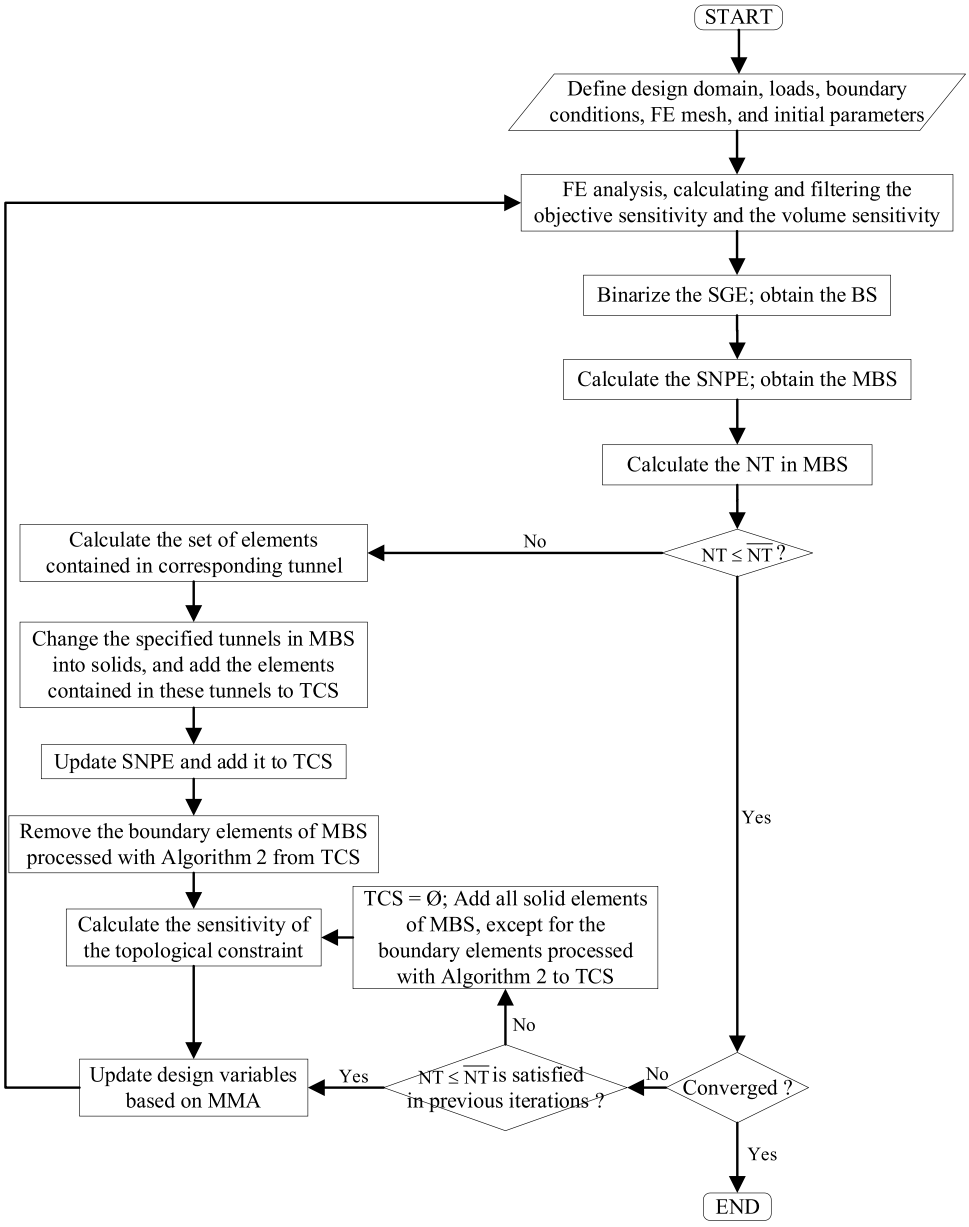

Fig. 12. Algorithm flow chart for control tunnel only.

control. Notably, in the optimization process, the optimized result of a certain iteration does not strictly satisfy the topological constraint, but the final optimized result is guaranteed to satisfy the topological constraint. The flowcharts of the algorithm controlling only the structural tunnel and cavity are shown in Figs. 12 and 13, respectively. The detailed optimization algorithm of topological control above can be expressed as follows:

a) Define the design domain, loads, boundary conditions, finite element mesh and initialization parameters.

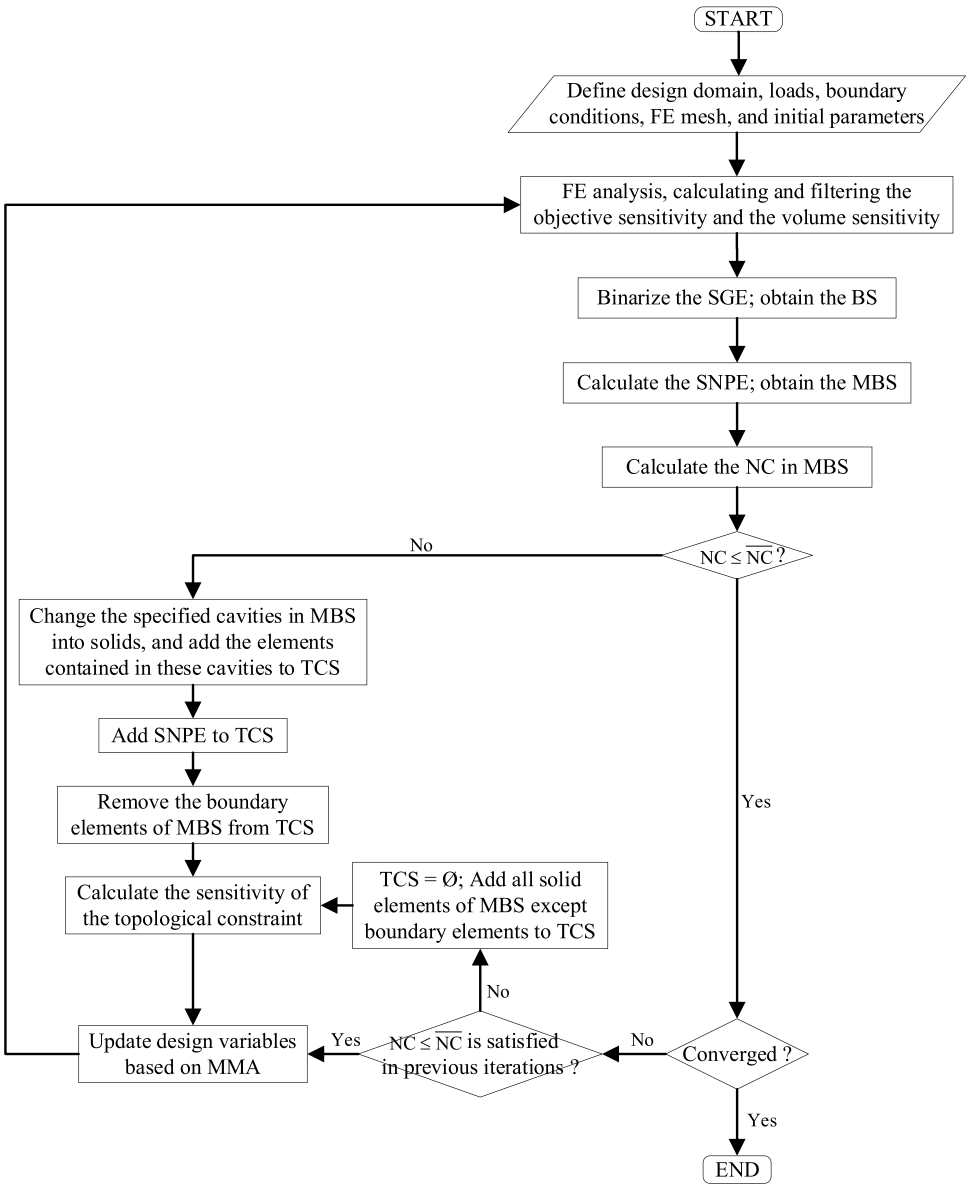

Fig. 13. Algorithm flow chart for control cavity only.

b) Finite element analysis, calculating and filtering the objective sensitivity and the volume sensitivity.
c) Binarize the SGE to obtain the BS.
d) Calculate the set of elements *SNPE* that need to be processed to remove nonmanifold points and nonmanifold edges, and then obtain the MBS.
e) If only the tunnel is controlled, the *NT* of the MBS is calculated.
f) If only the cavity is controlled, calculate the *NC* of the MBS and skip to step j).
g) If $NT \leq \overline{NT}$, end the optimization process if the optimization model converges.
h) If the optimization model does not converge, then determine if $NT \leq \overline{NT}$ is satisfied in the previous iterations; if not, then change the *TCS* to empty and add all solid elements in the MBS to the *TCS* except for the boundary elements processed with Algorithm 2, and skip to step n) if satisfied.
i) If $NT > \overline{NT}$, first calculate the set of elements contained in the tunnel ET_i, $1 \leq i \leq NT$. Then select the tunnels specified in the MBS and turn them into solids while adding the elements contained in these tunnels to *TCS*. Update *SNPE* and add it to *TCS*. Then the boundary elements of the MBS processed with Algorithm 2 are removed from the *TCS*.
j) If $NC \leq \overline{NC}$, end the optimization process if the optimization model converges.
k) If the optimization model does not converge, then determine if $NC \leq \overline{NC}$ is satisfied in the previous iterations; if not, then change the *TCS* to empty and add all the solid elements of the MBS except the boundary elements to *TCS*, and skip to step n) if satisfied.
l) If $NC > \overline{NC}$, select the cavities specified in the MBS and turn them into solids, then add the elements contained in these cavities to the *TCS*. Add the *SNPE* to the *TCS* and remove the solid boundary elements of the MBS from the *TCS*.
m) Calculate the sensitivity of the topological constraint.

n) Update the element design variables based on MMA.
o) Repeat steps b)–n) until the optimization model satisfies the constraints.

6. 3D numerical examples

Under the structural topological and volume constraints, the topology optimization model that minimizes structural compliance can be written in the following form:

$$\begin{aligned} &\text{Find } \boldsymbol{\rho} = (\rho_1, \rho_2, \ldots, \rho_n)^{\mathrm{T}} \\ &\text{Min } C(\boldsymbol{\rho}) = \boldsymbol{u}^{\mathrm{T}} \boldsymbol{K}(\boldsymbol{\rho}) \boldsymbol{u} \\ &\text{S.t. } \boldsymbol{K}(\boldsymbol{\rho}) \boldsymbol{u} = \boldsymbol{f} \\ &\quad V(\boldsymbol{\rho}) = \sum_{i=1}^{n} \rho_i v_i / \sum_{i=1}^{n} v_i \le \overline{\mathrm{V}} \\ &\quad tc(\boldsymbol{\rho}) = \sum_{j \in TCS} \left(\rho_j - 1\right)^2 \le \varepsilon \\ &\quad \rho_{\min} \le \rho_i \le 1, \forall i \in 1, 2, \ldots, n \end{aligned} \tag{15}$$

In Eq. (15), $\boldsymbol{\rho}$ is the vector of the design variables, with ρ_i and v_i denoting the density and volume of the ith element. n denotes the total number of finite elements used to discretize the prescribed design domain Ω. $\boldsymbol{K} = \sum_{i=1}^{n} \rho_i^p \boldsymbol{K}_0$ (p is the penalization index and $p = 3$ is adopted in the present study) is the global stiffness matrix, with $\boldsymbol{K}_0$ representing the element stiffness matrix corresponding to $\rho_i = 1$. $\rho_{min} = 0.001$ is the lower bound of the element density. $\overline{V}$ is the prescribed upper bound for solid material. $\boldsymbol{f}$ and $\boldsymbol{u}$ are the external load and displacement fields, respectively. $tc(\boldsymbol{\rho}) \le \varepsilon$ is a topological constraint, where TCS is defined in Eq. (11), and the value of ε is 0.001 in the numerical implementation.

Under the conditions of structural topological and volume constraints, the topology optimization model of the compliant mechanism problem can be expressed as follows:

$$\begin{aligned} &\text{Find } \boldsymbol{\rho} = (\rho_1, \rho_2, \ldots, \rho_n)^{\mathrm{T}} \\ &\text{Max } C(\boldsymbol{\rho}) = \boldsymbol{l}^{\mathrm{T}} \boldsymbol{u} \\ &\text{S.t. } \boldsymbol{K}(\boldsymbol{\rho}) \boldsymbol{u} = \boldsymbol{f} \\ &\quad V(\boldsymbol{\rho}) = \sum_{i=1}^{n} \rho_i v_i / \sum_{i=1}^{n} v_i \le \overline{\mathrm{V}} \\ &\quad tc(\boldsymbol{\rho}) = \sum_{j \in TCS} \left(\rho_j - 1\right)^2 \le \varepsilon \\ &\quad \rho_{\min} \le \rho_i \le 1, \forall i \in 1, 2, \ldots, n \end{aligned} \tag{16}$$

Where $\boldsymbol{u}$ and $\boldsymbol{f}$ are the solution and input vectors, respectively. The vector $\boldsymbol{l}$ takes a value of zero at all positions, except for the position corresponding to the output degree of freedom, which is set to one.

In this section, three 3D numerical examples of a bridge, cantilever beam, and compliant gripper are presented to demonstrate the effectiveness of the proposed algorithm. It should be noticed that the topological constraint is highly non-convex function of the design variables and the final optimization results are expected to be only local minima. Therefore, in order to prevent the topological constraint from hindering the formation of the appropriate load-carrying structural topology at initial stages of optimization, thus leading the optimization process into local minima prematurely, topological constraint should be added after certain iteration steps from numerical implementation point of view.

6.1. Bridge

In this example, we consider a 3D bridge. The model is illustrated in Fig. 14. At the top of the design domain is a thin non-designable deck. The finite-element mesh consists of $20 * 20 * 40$ hexahedral elements. The target volume fraction and filter radius are 0.4 and $\sqrt{3}$, respectively.

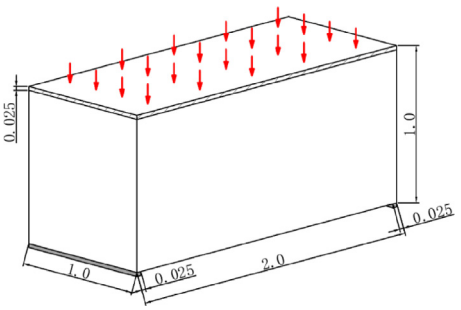

Fig. 14. Bridge model.

For comparison purposes, the classical compliance minimum problem without topological constraint is first solved, and the optimized structure is shown in Fig. 15, where the opaque (a), cross-sectional (b), semi-transparent with a set of shortest tunnel loops (red loops) (c), semi-transparent with non-shortest tunnel loops (blue loops) (d), and semi-transparent (e) versions of each structure are used for visualization. Fig. 15(f) shows the iterative curves of the objective function, NT and NC, where the objective function value, NT and NC are 15.73, 4 and 2, respectively. As shown in Fig. 15(f), there is a large NT in the early stages of topology optimization (first 20 iteration steps), and one of the reasons for this phenomenon in our analysis is the large gray area at projection. In addition, a better topology has not been developed in the early stages of optimization, thus to avoid falling into a local minimum prematurely, in this case we added topological constraint after the 20th step. Subsequently, three different topological control modes are solved under the same conditions. The first controls only the structural tunnel, given $\overline{NT} = 0$. Fig. 16 shows the corresponding optimized structure with the objective function values, NT and NC values of 15.96, 0 and 2, respectively. The second controls only the structural cavity, given the $\overline{NC} = 0$. Fig. 17 shows the corresponding optimized structure with the objective function values, NT and NC values of 16.04, 4 and 0, respectively. The third is to control both the structural tunnel and cavity, given $\overline{NT} = 0, \overline{NC} = 0$. Fig. 18 illustrates the corresponding optimized structure with the objective function values, NT and NC values of 16.04, 0 and 0, respectively. In addition, the objective function values of the above optimization results with topological constraint are smaller than that of the original optimization result, which indicates that the topological constraint is satisfied at the expense of the objective function value.

6.2. Cantilever beam

The second example considers a cantilever beam. The sizes of the design domain and boundary conditions are shown in Fig. 19. The finite-element mesh consists of $30 \times 45 \times 90$ elements. The target volume fraction and filter radius are 0.12 and $\sqrt{3}$, respectively. For comparison purposes, the classical compliance minimum problem without topological constraint is first solved, and the optimized structure is shown in Fig. 20, where the opaque (a), semi-transparent (b), and semi-transparent with a set of shortest tunnel loops (red loops) are arranged in ascending order according to the length and symmetry of the tunnel loops (c)–(h). Further, the semi-transparent with non-shortest tunnel loop (blue loop) (i) versions of each structure are used for visualization. For the structure with $NT = 10, NC = 0$. Next, the same problem is solved using the optimization model in Eq. (15) with $\overline{NT} = 0, 1, 2, 3, 4, 5, 6, 7$. Figs. 21–28 show the corresponding optimized results.

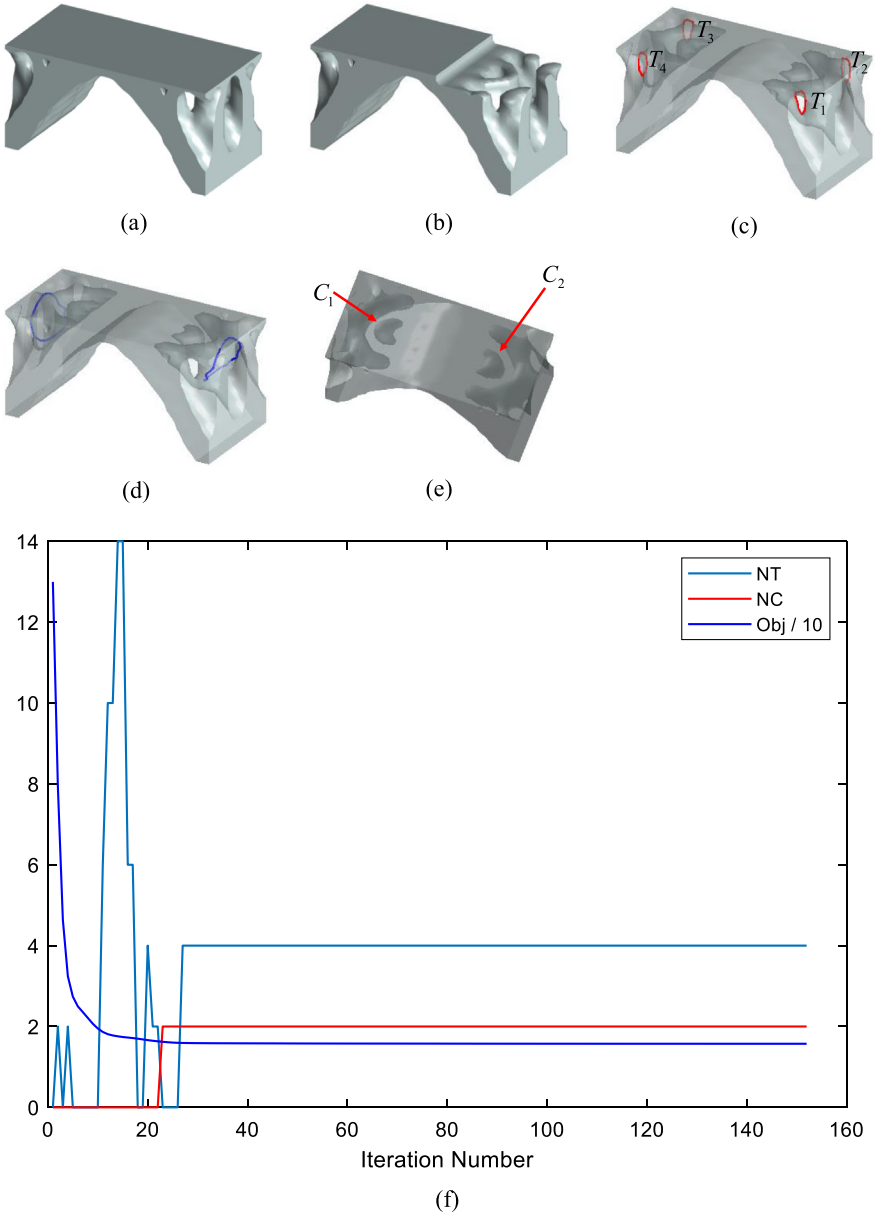

Fig. 15. Optimized result without topological constraint, where opaque (a), cross-sectional (b), semi-transparent with a set of shortest tunnel loops (red loops) (c), semi-transparent with non-shortest tunnel loops (blue loops) (d) and semi-transparent (e) versions of each structure are used for visualization. (f) Iteration curves of the objective function, *NT* and *NC*, where the objective function value, *NT* and *NC* of the optimization result are 15.73, 4 and 2, respectively. (For interpretation of the references to color in this figure legend, the reader is referred to the web version of this article.)

6.3. Compliant gripper

The third example is a 3D compliant gripper, a quarter of which is shown in Fig. 29. The finite-element mesh consists of $30 \times 30 \times 40$ elements. An input load $f = 1$ is applied at the center point of the left-side surface. The input spring stiffness $k_{in} = 10$, and the output spring stiffness is $k_{out} = 10$. The target volume fraction and filter radius are 0.05 and $\sqrt{3}$, respectively. Owing to the symmetrical property, only a quarter of the design domain is analyzed with a finite element. Topology analysis is conducted on the entire design domain. For comparison, the complaint mechanism problem without topological constraint is first solved, and the optimized structure is shown in Fig. 30, where the versions of the opaque (a), semi-transparent (b), semi-transparent with a set of shortest tunnel loops (red loops) and arranged in ascending order according to the length and symmetry of the tunnel loops (c)–(g), and semi-transparent with the non-shortest tunnel loop (blue loop) (h) structure are used for visualization. For the structure with $NT = 10, NC = 0$. Next, the same problem is solved using the optimization model in Eq. (16) with $\overline{NT} = 0, 1, 2$, respectively. Figs. 31–33 show the corresponding optimized results.

7. Conclusion

In this study, a method is proposed to explicitly and quantitatively control the topology of a 3D structure. The method was successfully integrated into the computational framework of the SIMP interpolation and MMA optimization algorithm. Numerical examples demonstrate that the maximum number of structural

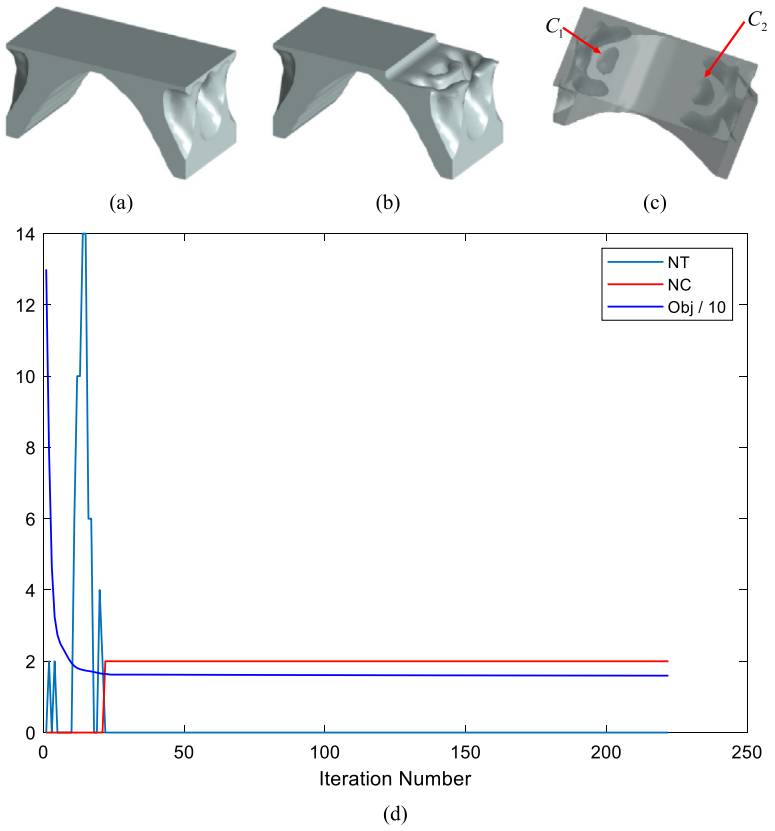

Fig. 16. Optimized result with $\overline{NT} = 0$, where opaque (a), cross-sectional (b), and semi-transparent (c) versions of each structure are used for visualization. (d) Iteration curves of the objective function, *NT* and *NC*, where the objective function value, *NT* and *NC* of the optimization result are 15.96, 0 and 2, respectively.

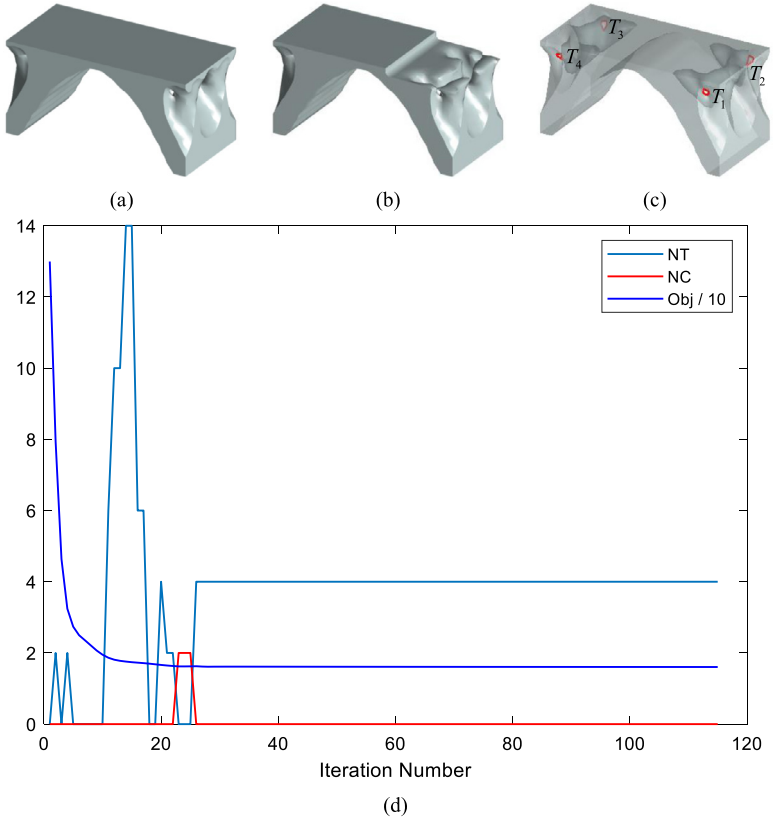

Fig. 17. Optimized result with $\overline{NC} = 0$, where opaque (a), cross-sectional (b), and semi-transparent (with a set of shortest tunnel loops (red loops)) (c) versions of each structure are used for visualization. (d) Iteration curves of the objective function, *NT* and *NC*, where the objective function value, *NT* and *NC* of the optimization result are 16.04, 4 and 0, respectively. (For interpretation of the references to color in this figure legend, the reader is referred to the web version of this article.)

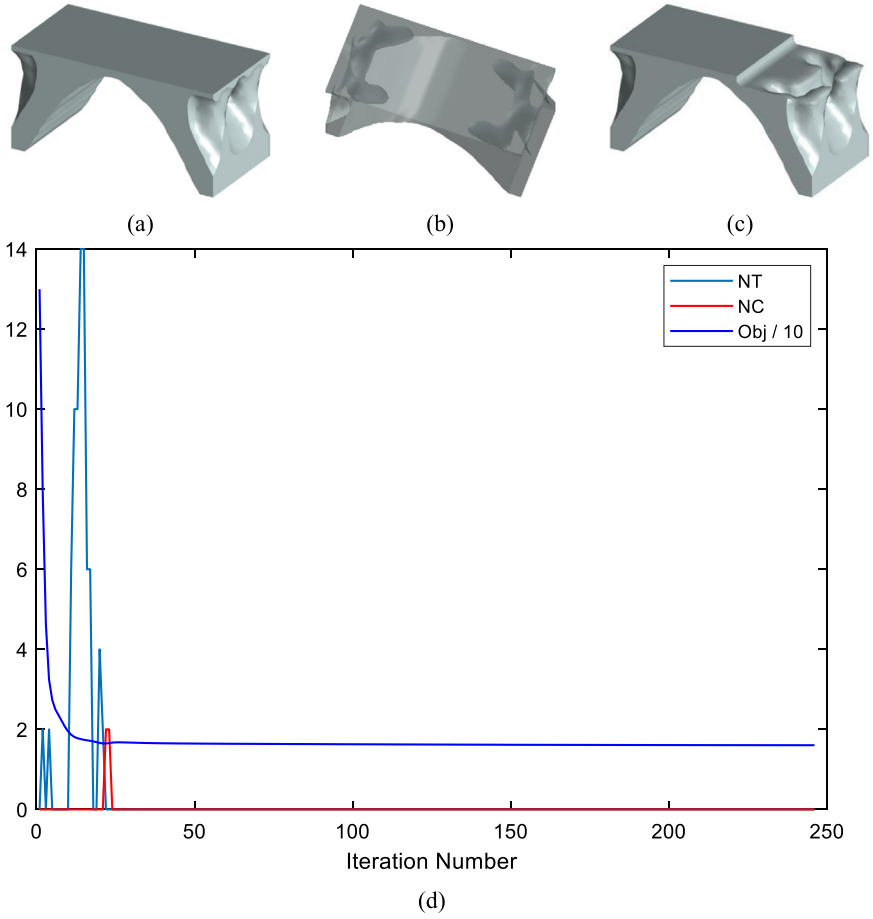

Fig. 18. Optimized result with $\overline{NT} = 0, \overline{NC} = 0$, where opaque (a), semi-transparent (b), and cross-sectional versions of each structure are used for visualization. (d) Iteration curves of the objective function, *NT* and *NC*, where the objective function value, *NT* and *NC* of the optimization result are 16.04, 0 and 0, respectively.

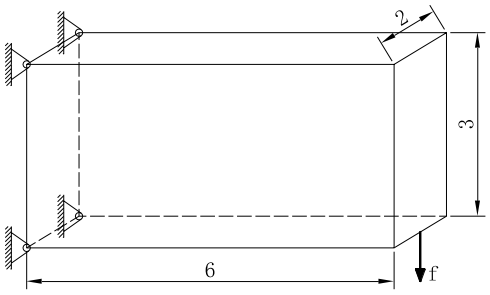

Fig. 19. Cantilever beam model.

tunnels and cavities can be quantitatively controlled using this method to control the structural topology.

In this paper, only the control of cavities and tunnels in 3D structures is discussed, but the control of independent connected components deserves further study. In this study, the characteristic information of tunnel is calculated by using the tunnel loop of homology theory, and the *NT* of structure is reduced by filling the tunnel loop. We believe that the characteristic information of structural tunnel can also be obtained from the skeleton of the structure, as well as the *NT* of the structure can be reduced by cutting the handle loop. In addition, the efficient computation of the shortest tunneling loop with repeatability is worth further study. From a manufacturing and assembly point of view, it is worthwhile to control the shape and size of the holes and rods when controlling the topology of the structure.

Declaration of competing interest

The authors declare that they have no known competing financial interests or personal relationships that could have appeared to influence the work reported in this paper.

Data availability

The authors do not have permission to share data.

Acknowledgments

This research was supported by the National Natural Science Foundation of China Grant Number51675506. We would like to thank Prof. Svanberg for the MMA algorithm.

Replication of results

On behalf of all authors, the corresponding author states that the results presented in this paper can be reproduced by the implementation details provided herein.

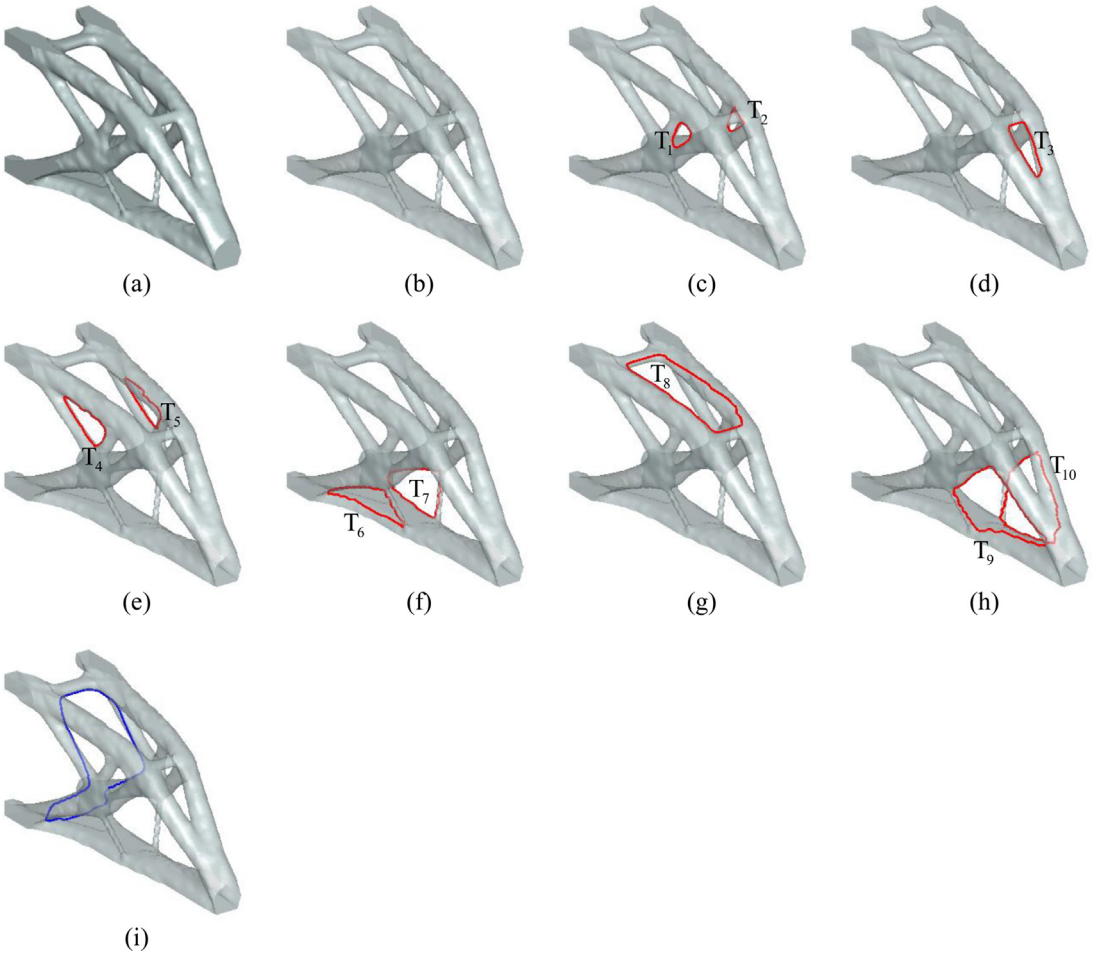

Fig. 20. Optimized result without topological constraint, where opaque (a), semi-transparent (b), semi-transparent with a set of shortest tunnel loops (red loops) (c)–(h), and semitransparent (with non-shortest tunnel loop) (blue loop) (i) versions of each structure are used for visualization. The structure has 10 tunnels ($NT = 10$) and 0 cavities ($NC = 0$). The objective function value of the optimized result is 78.95. (For interpretation of the references to color in this figure legend, the reader is referred to the web version of this article.)

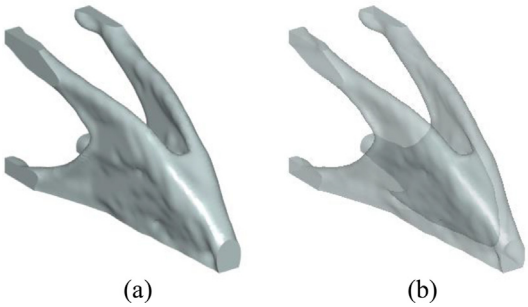

Fig. 21. Optimized result with $\overline{\mathrm{NT}} = 0$, where opaque (a) and semitransparent (b) versions of each structure are used for visualization. The structure has zero tunnels ($NT = 0$) and zero cavities ($NC = 0$). The objective function value of the optimized result is 85.20.

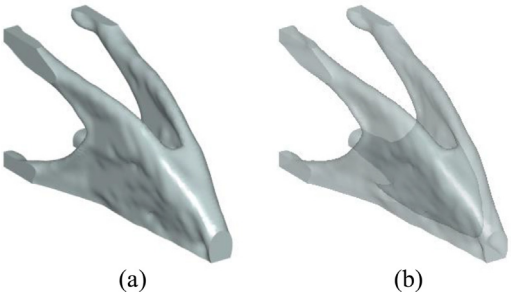

Fig. 22. Optimized result with $\overline{NT} = 1$, where opaque (a) and semi-transparent (b) versions of each structure are used for visualization. The structure has zero tunnels ($NT = 0$) and zero cavities ($NC = 0$). The objective function value of the optimized result is 85.20.

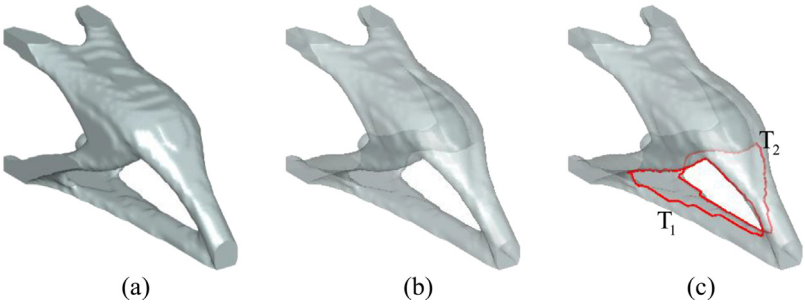

Fig. 23. Optimized result with $\overline{NT} = 2$, where opaque (a), semitransparent (b) and semitransparent (with a set of shortest tunnel loops) (red loops) (c) versions of each structure are used for visualization. The structure has two tunnels ($NT = 2$) and zero cavities ($NC = 0$). The objective function value of the optimized result is 80.40. (For interpretation of the references to color in this figure legend, the reader is referred to the web version of this article.)

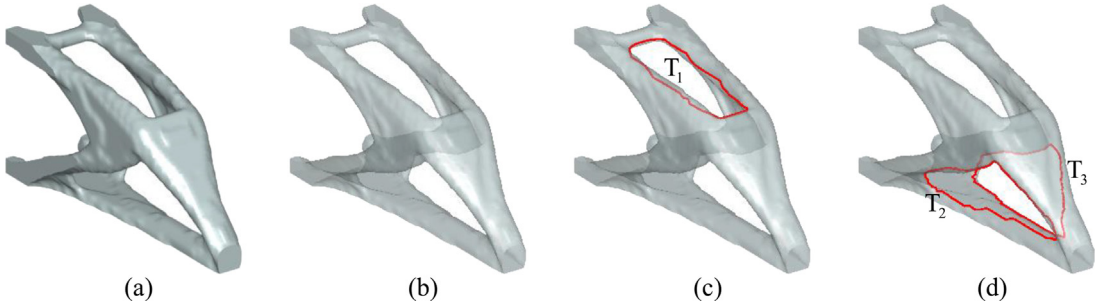

Fig. 24. Optimized result with $\overline{NT} = 3$, where opaque (a), semi-transparent (b), and semi-transparent (with a set of shortest tunnel loops) (red loops) (c)–(d) versions of each structure are used for visualization. The structure has three tunnels ($NT = 3$) and zero cavities ($NC = 0$). The objective function value of the optimized result is 80.13. (For interpretation of the references to color in this figure legend, the reader is referred to the web version of this article.)

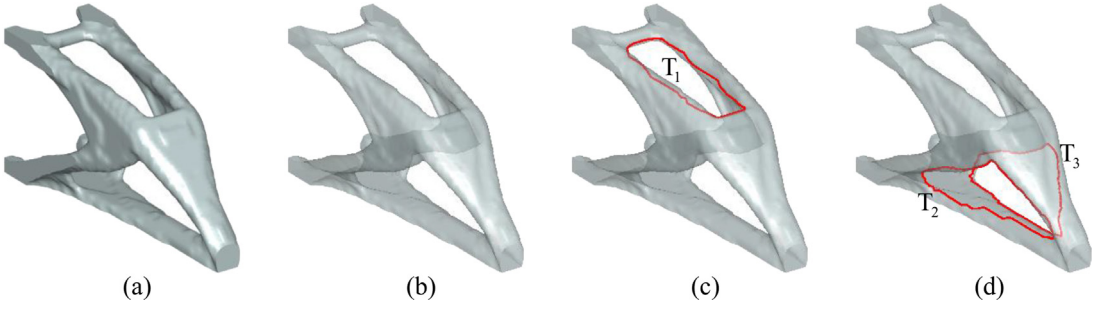

Fig. 25. Optimized result with $\overline{NT} = 4$, where opaque (a), semi-transparent (b) and semi-transparent (with a set of shortest tunnel loops) (red loops) (c)–(d) versions of each structure are used for visualization. The structure has three tunnels ($NT = 3$) and zero cavities ($NC = 0$). The objective function value of the optimized result is 80.13. (For interpretation of the references to color in this figure legend, the reader is referred to the web version of this article.)

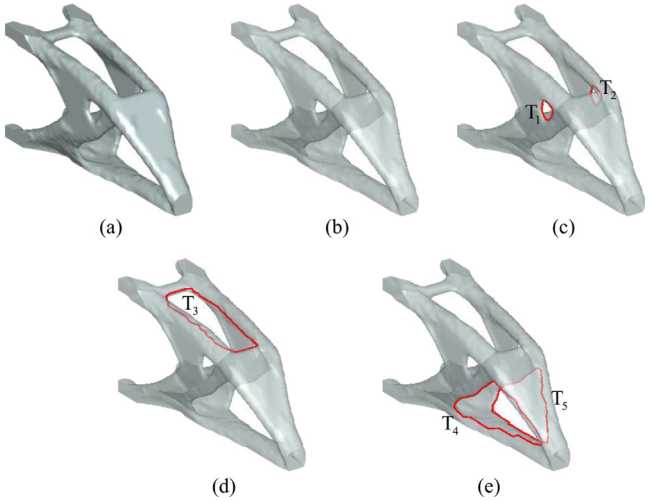

Fig. 26. Optimized result with $\overline{NT} = 5$, where opaque (a), semi-transparent (b) and semi-transparent (with a set of shortest tunnel loops) (red loops) (c)–(e) versions of each structure are used for visualization. The structure has five tunnels ($NT = 5$) and zero cavities ($NC = 0$). The objective function value of the optimized result is 80.58. (For interpretation of the references to color in this figure legend, the reader is referred to the web version of this article.)

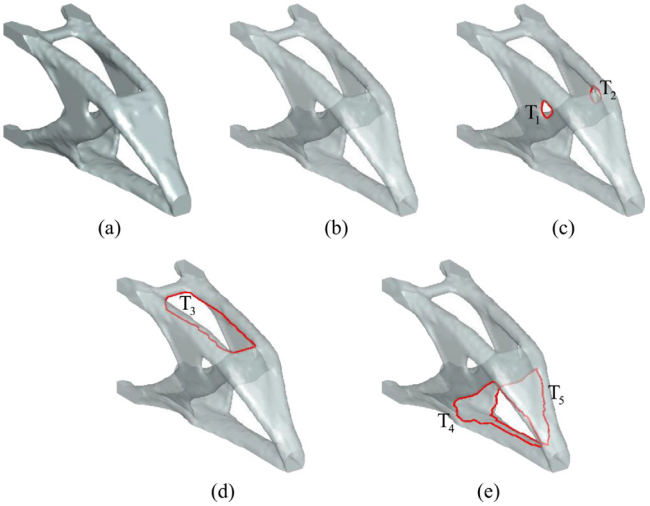

Fig. 27. Optimized result with $\overline{NT} = 6$, where opaque (a), semi-transparent (b) and semi-transparent (with a set of shortest tunnel loops) (red loops) (c)–(e) versions of each structure are used for visualization. The structure has five tunnels ($NT = 5$) and zero cavities ($NC = 0$). The objective function value of the optimized result is 80.58. (For interpretation of the references to color in this figure legend, the reader is referred to the web version of this article.)

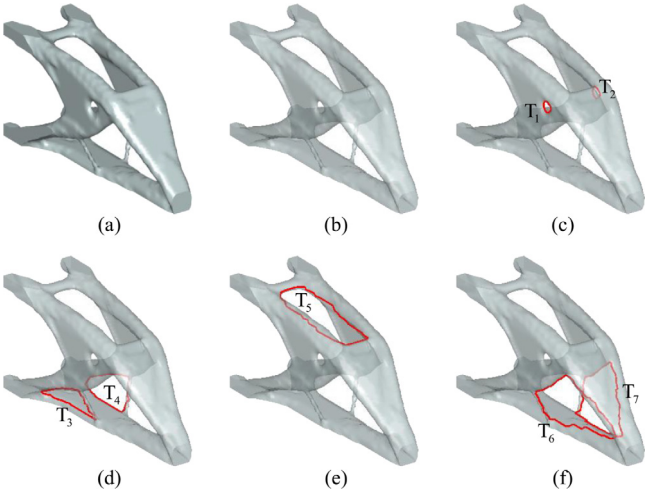

Fig. 28. Optimized result with $\overline{NT} = 7$, where opaque (a), semi-transparent (b) and semi-transparent (with a set of shortest tunnel loops) (red loops) (c)–(f) versions of each structure are used for visualization. The structure has five tunnels ($NT = 7$) and zero cavities ($NC = 0$). The objective function value of the optimized result is 79.64. (For interpretation of the references to color in this figure legend, the reader is referred to the web version of this article.)

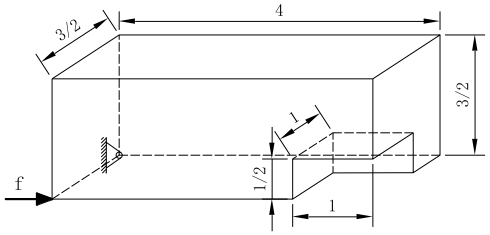

Fig. 29. Compliant gripper model.

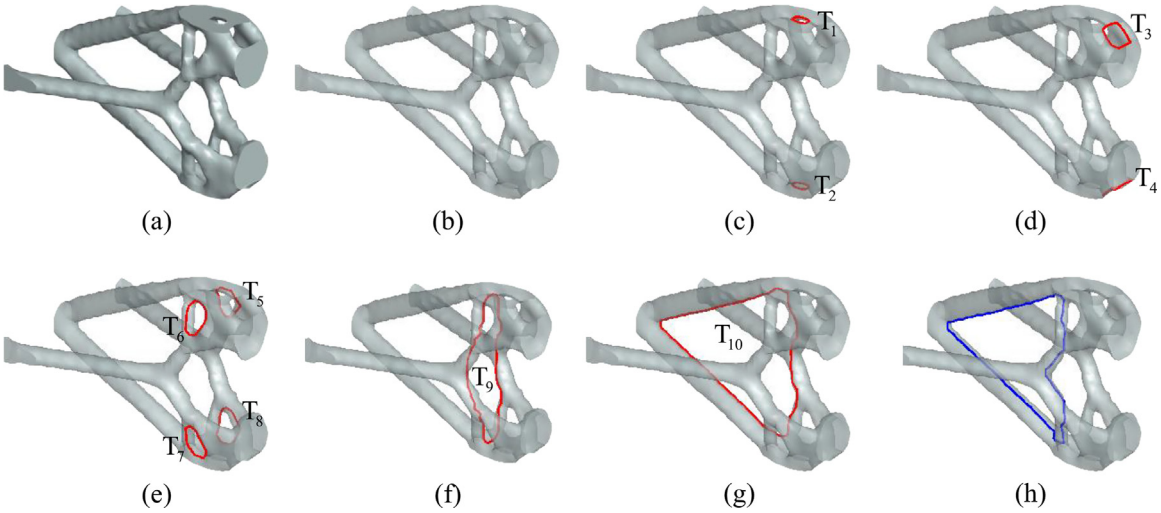

Fig. 30. Optimized result without topological constraint, where the versions of opaque (a), semi-transparent (b), semi-transparent with a set of shortest tunnel loops (red loops) (c)–(g), and semi-transparent with non-shortest tunnel loop (blue loop) (h) structures are used for visualization. The structure has 10 tunnels ($NT = 10$) and 0 cavities ($NC = 0$). The objective function value of the optimized result is 0.70. (For interpretation of the references to color in this figure legend, the reader is referred to the web version of this article.)

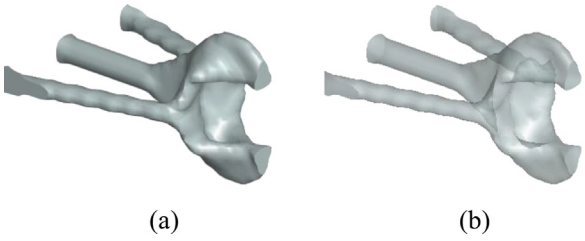

Fig. 31. Optimized result for $\overline{NT} = 0$, where opaque (a) and semi-transparent (b) versions of each structure are used for visualization. The structure has zero tunnels ($NT = 0$) and zero cavities ($NC = 0$). The objective function value of the optimized result is 0.18.

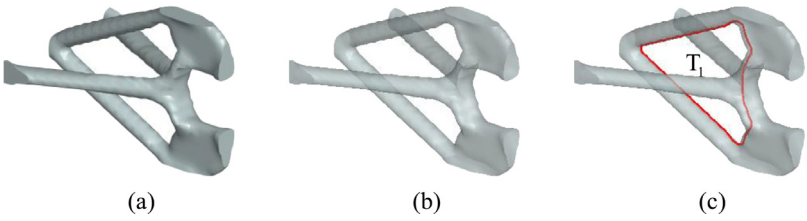

Fig. 32. Optimized result with $\overline{NT} = 1$, where the versions of opaque (a), semi-transparent (b), and semi-transparent with a set of shortest tunnel loop (red loop) (c) structures are used for visualization. The structure has one tunnel ($NT = 1$) and zero cavities ($NC = 0$). The objective function value of the optimized result is 0.82. (For interpretation of the references to color in this figure legend, the reader is referred to the web version of this article.)

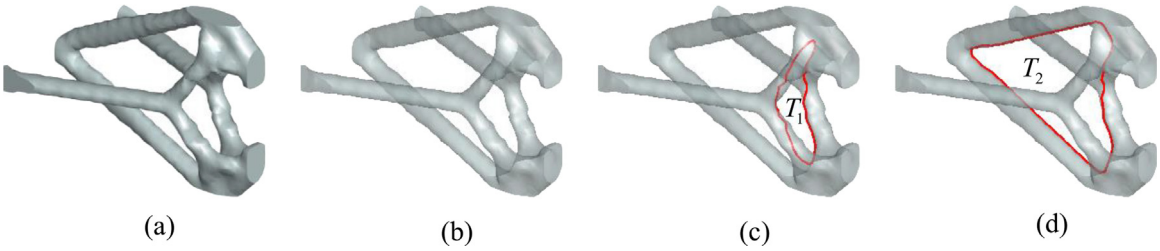

Fig. 33. Optimized result with $\overline{NT} = 2$, where versions of opaque (a), semi-transparent (b), and semi-transparent with a set of shortest tunnel loops (red loops) (c)–(d) structures are used for visualization. The structure has two tunnels ($NT = 2$) and zero cavities ($NC = 0$). The objective function value of the optimized result is 0.71. (For interpretation of the references to color in this figure legend, the reader is referred to the web version of this article.)

References

[1] Bendsøe MP, Kikuchi N. Generating optimal topologies in structural design using a homogenization method. Comput Methods Appl Mech Engrg 1988;71:197–224.
[2] Bendsøe MP, Sigmund O. Material interpolation schemes in topology optimization. Arch Appl Mech 1999;69:635–54.
[3] Xie YM, Steven GP. A simple evolutionary procedure for structural optimization. Comput Struct 1993;49:885–96.
[4] Wang MY, Wang X, Guo D. A level set method for structural topology optimization. Comput Methods Appl Mech Engrg 2003;192:227–46.
[5] Guo X. Doing topology optimization explicitly and geometrically: A new moving morphable components based framework. 2014, p. 31–2.
[6] Liang Y, Cheng G. Topology optimization via sequential integer programming and canonical relaxation algorithm. Comput Methods Appl Mech Engrg 2019;348:64–96.
[7] Liang Y, Yan X, Cheng G. Explicit control of 2D and 3D structural complexity by discrete variable topology optimization method. Comput Methods Appl Mech Engrg 2021;114302.
[8] Bendsøe M, Sigmund O. Topology optimization: Theory, method and applications. 2003.
[9] Kruth JP, Mercelis P, Van Vaerenbergh J, Froyen L, Rombouts M. Binding mechanisms in selective laser sintering and selective laser melting. Rapid Prototyp J 2005;11:26–36.
[10] Zein I, Hutmacher DW, Tan KC, Teoh SH. Fused deposition modeling of novel scaffold architectures for tissue engineering applications. Biomaterials 2002;23:1169–85.
[11] Bourdin B. Filters in topology optimization. Internat J Numer Methods Engrg 2001;50:2143–58.
[12] Sigmund O. Design of material structures using topology optimization. 1994.
[13] Kim H, Querin OM, Steven GP, Xie YM. A method for varying the number of cavities in an optimized topology using evolutionary structural optimization. Struct Multidiscip Optim 2000;19:140–7.
[14] Zhang W, Zhong W, Guo X. An explicit length scale control approach in SIMP-based topology optimization. Comput Methods Appl Mech Engrg 2014;282:71–86.
[15] Zhou M, Lazarov BS, Wang F, Sigmund O. Minimum length scale in topology optimization by geometric constraints. Comput Methods Appl Mech Engrg 2015;293:266–82.
[16] lu Z, Zhang W. Topology optimization method with elimination of enclosed voids. Struct Multidiscip Optim 2019;60.
[17] Li Q, Chen W, Liu S, Fan H. Topology optimization design of cast parts based on virtual temperature method. Comput Aided Des 2018;94:28–40.
[18] Liu S, Li Q, Chen W, Tong L, Cheng G. An identification method for enclosed voids restriction in manufacturability design for additive manufacturing structures. Front Mech Eng 2015;10:126–37.
[19] Yamada T, Noguchi Y. Topology optimization with a closed cavity exclusion constraint for additive manufacturing based on the fictitious physical model approach. Addit Manuf 2022;52:102630.
[20] Han H, Guo Y, Chen S, Liu Z. Topological constraints in 2D structural topology optimization. Struct Multidiscip Optim 2021;63:39–58.
[21] Xiong Y, Yao S, Zhao ZL, Xie YM. A new approach to eliminating enclosed voids in topology optimization for additive manufacturing. Addit Manuf 2020;32:101006.
[22] Zhao ZL, Zhou S, Cai K, Min Xie Y. A direct approach to controlling the topology in structural optimization. Comput Struct 2020;227:106141.
[23] Zhao ZL, Zhou S, Feng XQ, Xie YM. Morphological optimization of scorpion telson. J Mech Phys Solids 2020;135:103773.
[24] He Y, Zhao ZL, Cai K, Kirby J, Xiong Y, Xie YM. A thinning algorithm based approach to controlling structural complexity in topology optimization. Finite Elem Anal Des 2022;207:103779.
[25] Liang Y, Cheng G. Further elaborations on topology optimization via sequential integer programming and canonical relaxation algorithm and 128-line MATLAB code. Struct Multidiscip Optim 2020;61:411–31.
[26] Han H, Wang C, Zuo T, Liu Z. Inequality constraint on the maximum genus for 3D structural compliance topology optimization. Sci Rep 2022;12:16185.
[27] Wang Q, Han H, Wang C, Liu Z. Topological control for 2D minimum compliance topology optimization using SIMP method. Struct Multidiscip Optim 2022;65:38.
[28] Zuo T, Wang C, Han H, Wang Q, Liu Z. Explicit 2D topological control using SIMP and MMA in structural topology optimization. Struct Multidiscip Optim 2022;65:293.
[29] Svanberg K. The method of moving asymptotes—A new method for structural optimization. Internat J Numer Methods Engrg 2010;24:359–73.
[30] Mäntylä M. Boolean operations of 2-manifolds through vertex neighborhood classification. ACM Trans Graph 1986;5.
[31] Requicha AAG, Voelcker HB. Solid modeling: Current status and research directions. IEEE Comput Graph Appl 1983;3:25–37.
[32] Poulsen T. A simple scheme to prevent checkerboard patterns and one-node connected hinges in topology optimization. Struct Multidiscip Optim 2002;24:396–9.
[33] Homology, topology and its applications. 2006, p. 269–311.
[34] Dey T, Fan F, Wang Y. An efficient computation of handle and tunnel loops via Reeb graphs. ACM Trans Graph 2013;32.
[35] Li L, Khandelwal K. Volume preserving projection filters and continuation methods in topology optimization. Eng Struct 2015;85:144–61.
[36] Guest JK, Asadpoure A, Ha SH. Eliminating beta-continuation from heaviside projection and density filter algorithms. Struct Multidiscip Optim 2011;44:443–53.
[37] Wang F, Lazarov BS, Sigmund O. On projection methods, convergence and robust formulations in topology optimization. Struct Multidiscip Optim 2011;43:767–84.
[38] Guest JK, Prévost JH, Belytschko T. Achieving minimum length scale in topology optimization using nodal design variables and projection functions. Internat J Numer Methods Engrg 2004;61:238–54.
[39] Ferrari F, Sigmund O. A new generation 99 line Matlab code for compliance topology optimization and its extension to 3D. Struct Multidiscip Optim 2020;62:2211–28.
[40] Xu S, Cai Y, Cheng G. Volume preserving nonlinear density filter based on heaviside functions. Struct Multidiscip Optim 2010;41:495–505.
[41] Dey TK, Li K, Sun J. On computing handle and tunnel loops. In: 2007 International Conference on Cyberworlds. CW'07, 2007, p. 357–66.
[42] Liepa P. Filling holes in meshes. 2003.